



Effects of climate change on lake area and vegetation cover over the past 55 years in Northeast Inner Mongolia grassland, China

Yanfei Zhang¹ · Wentao Liang¹ · Zilong Liao¹ · Zhenhua Han¹ · Xiaomin Xu¹ · Rui Jiao¹ · Hualin Liu¹

Received: 22 May 2018 / Accepted: 29 January 2019 / Published online: 13 February 2019
© Springer-Verlag GmbH Austria, part of Springer Nature 2019

Abstract

Previous studies indicate that vegetation and lakes in arid and semi-arid regions are closely related to climate change. However, the responses of vegetation and lakes to climate-related variables have rarely been contrastively studied. The Hulun Lake (HLL) and its surrounding grasslands in Northeast Inner Mongolia of China comprise a semi-arid region that has experienced intense climate change over the last several decades. This study aims to understand the key factors that control the variations in the lake area and vegetation cover over the last five decades in the HLL region, as well as contrastively investigate the different responses of the lake area and vegetation cover to climate-related variables. Analysis results indicate that the variations with increasing change rates in the HLL area were mainly controlled by precipitation fluctuation. Moreover, an increase or decrease in the air temperature and relative humidity could affect the response time of the HLL area to the change in precipitation. The Normalized Difference Vegetation Index (NDVI) variations from 1990 to 1999 around the HLL region were mainly controlled by the intense local grazing rather than climatic restrictions. The fluctuation in NDVI after 1999 reflects the response of the vegetation cover to climatic change. The correlation analysis shows that the variations in the HLL area were closely related to the multi-year tendency of precipitation amount and to the Standardized Precipitation Evapotranspiration Index (SPEI) with a long timescale. However, NDVI is sensitive to changes in short-term precipitation amount, such as seasonal precipitation, and in SPEI with a monthly timescale. The soil moisture at shallow depths (< 0.1 m) was the key root-zone soil moisture that could influence NDVI, whereas soil moisture at depths of 0.4 to 1.0 m and the HLL area were closely related and had similar responses to climatic change.

1 Introduction

Global climate has greatly changed in recent 100 years, and this change has exerted significant impacts on the hydrological cycle and ecological environment (Qin et al. 2005). Lakes act as the essential components of the hydrological cycle, especially for the lakes in the arid areas, which provide sparse but valuable water resources for the fragile environments and human beings (Bai et al. 2011). Climate change has resulted in a significant effect on the quantity and area of lakes during the past decades (e.g., Bai et al. 2011; Karlsson et al. 2014; Kang et al. 2015; Im et al. 2015; Cai et al. 2016; Xing et al. 2018).

Lake volumes could undergo large fluctuations because of various water inputs and outputs caused by changes in climate-related parameters; these fluctuations should be considered in future hydroclimatic and hydrological studies (Vallet-Coulomb et al. 2001; Kaiser et al. 2015). Heavy precipitation and low temperature are typically favorable to increase the lake volume in any temporal and spatial scales. The trend of decreasing lake area extended from the eastern to the western part of the arid regions of central Asia during the past 30 years, and this trend of lake changes was correlated to the variations of the spatial-temporal distribution in precipitation (Bai et al. 2011). The ultimate effect of continued climate warming on high-latitude, permafrost-controlled lakes and wetlands may be their widespread disappearance because permafrost influences substrate permeability and lake drainage (Smith et al. 2005). Warming monsoon and post-monsoon air temperatures enhanced the glacial lake surface area by contributing glacier melt water to the lakes in the last few decades (Ashraf et al. 2017; Yang et al. 2017; Debnath et al. 2018; Jing et al. 2018). Thermokarst lakes are also significantly amplified by climatic warming and permafrost degradation

✉ Yanfei Zhang
zhangyanfeigeo@163.com

¹ Institute of Water Resource for Pastoral Area, Ministry of Water Resources of the People's Republic of China, Hohhot 010020, Inner Mongolia, China

and erosion (Jones et al. 2011; Polishchuk and Sharonov 2013; Olthof et al. 2015; Nitze et al. 2017). Several studies comprehensively analyzed the effects of climate and human activities on lake changes (Wang et al. 2014; Fang et al. 2018; Jing et al. 2018). Increases in lake area occurred mainly in the less populated mountainous areas caused by glacier melting and increase in precipitation. Conversely, lakes in the densely populated regions decreased, which was significantly related to the increasing intensity of human activities (e.g., irrigation and surface water regulation) (Wang et al. 2014; Fang et al. 2018; Yao et al. 2018). The decrease has been particularly pronounced since the late 1990s in Inner Mongolia, and the number of lakes $> 10 \text{ km}^2$ has declined by 30% because of precipitation reduction and intensive human activities (Tao et al. 2015).

The distribution and coverage of natural vegetation are also known to be strongly influenced by climate change (Prentice 2001; Tucker et al. 2001; Gong and Ho 2003; Gong and Shi 2004; Wang et al. 2003; Piao et al. 2006; Bao et al. 2014). As focal factors, temperature and precipitation can influence the start and end of growing period and vegetation activity. A previous study indicated that the annual maximum NDVI showed an increasing trend in China over the last 16 years with increasing temperature (Zhang et al. 2017). Sun et al. (2010) has suggested the change of NDVI is consistent with the precipitation variation in Inner Mongolia of China. Both lake and vegetation dynamics are closely related to climate-related variables, and they can be important proxy indicators of current climatic change on a global or regional scale. Previous studies researched vegetation–climate and lake–climate relationships separately, and few studies focused on the different responses of vegetation and lakes to climate change. Thus, this study presents a contrastive analysis to understand the difference between the responses of vegetation dynamics and lake volume fluctuation to temporal changes in long-term climatic conditions and to examine the possible means by which climate affects vegetation and lake performances.

2 Description of the study area

2.1 Geography and geology

The study area is located on the eastern side of the border between the Mongolian People's Republic and the northeastern Inner Mongolia of China (Fig. 1). The study area, including Hulun Lake (HLL) and its surrounding grasslands, is totally about 7400 km^2 in size. This area was designated a Provincial Nature Reserve in 1990, approved as a National Nature Reserve in 1992 (Li et al. 2013). The protection of our study area can effectively decrease the influence of human activities when vegetation–climate and lake–climate relationships are discussed. HLL is located within the lowest portion of the

NE-trending and down-faulted Hailaer basin. The topography of HLL area is high in the northwest and low in the southeast, with altitudes varying from 450 to 1125 m (Fig. 1). A hilly belt with NE-trending and widely lacustrine plain is a main landform in the northwest and southeast side of lakeshore, respectively. The igneous rocks including extrusive rock of Jurassic basalt, rhyolite, and andesite and Jurassic–Cretaceous granites are widely distributed in the northwest side of study area. Thick alluvial and eolian deposits are mainly distributed in the southeast side of study area (Xu et al. 1989).

2.2 Hulun Lake and rivers

HLL, the fifth largest lake in China, is part of the Argun River water system. It provides very important water resources for the fragile environment and ecosystem in Hulun Buir Grassland. The HLL has a maximum water depth of $\sim 8 \text{ m}$ when the elevation of the lake level is 545.4 m a.s.l. in June of 1968 (measurements in the period of 1959 to 1981). HLL is mainly supplied by precipitation as well as by several rivers including the Kelulun River, the Wuerxun River, and the Xinkai River (Li et al. 2013; Fig. 1). Lake water consumption by local human activities is small ($73,000$ to $146,000 \text{ m}^3/\text{a}$) relative to the 3.3 billion m^3 to 14.0 billion m^3 (lake area 1609.6 to 2406 km^2) of water volume in HLL. Lake water leakage is weak because of the 0.5-m -thick sludge in the lake bed (Xu et al. 1989).

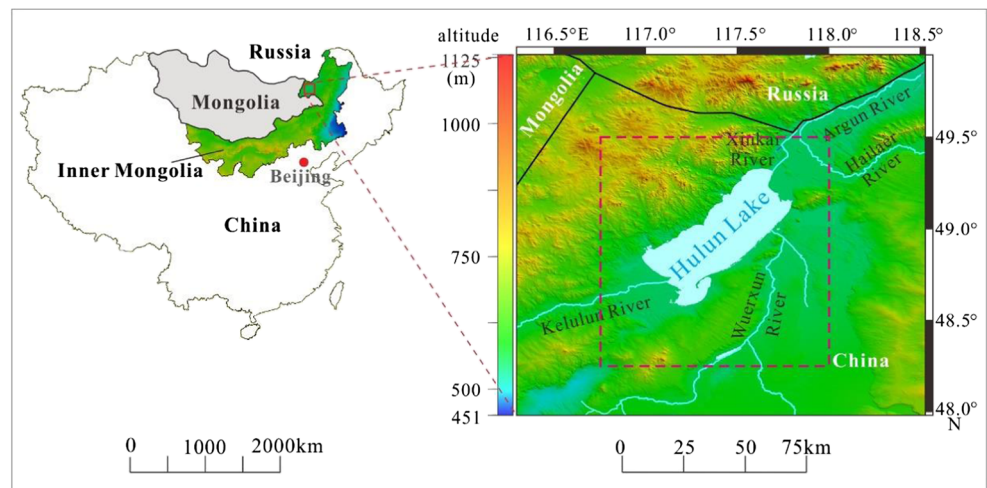
2.3 Climate

The study area lies in the northeast of Hulun Buir Grassland which has a continental monsoon climate with the middle latitude temperate zone and a cold temperate zone which leads to lower temperatures, a bigger temperature range, and violent summer and winter changes, resulting being one of the cold regions in China. Hulun Buir Grassland has experienced dramatic climate change, which has been more pronounced than most other areas in China over recent decades (Qian and Lin 2004; Lu et al. 2009). Most of the area in Hulun Buir Grassland has an arid to semi-arid climate, and the ecological environment in this district is fragile and sensitive to global climate change. In the study region, mean annual evaporation reaches $1400\text{--}1900 \text{ mm}$, which is five to six times the annual precipitation (Xiao et al. 2009). The lake is covered with ice from early November to late April.

3 Datasets and method

Data from Hailaer meteorological station in the lake region were used in this study. Meteorological data include daily precipitation, mean temperature, and relative humidity duration from 1960 to 2015.

Fig. 1 Location of Hulun Lake. Red dashed line: the study area of NDVI and soil moisture around Hulun Lake



Landsat MSS, TM, ETM+, and OLI imageries during 1973–2015 were used as remote sensing data source for investigating lake extent variations in the study area. A total of 53 usable Landsat images were processed to identify and measure the HLL area by using ENVI and ArcGIS software. The Landsat images with cloud coverage of less than 10% and acquired in summer and autumn were preferentially selected to be downloaded from USGS GLOVIS. Several Landsat images in spring and winter without snow cover were selected because of the high cloud and haze coverage in summer and autumn. The spatial resolution ($79 \text{ m} \times 57 \text{ m}$, although resampled to 60 m during level 1 processing) of the MSS imagery is lower than those of the TM, ETM+, and OLI imageries (30 m for the bands used for water extraction). In contrast to Landsat TM, ETM+, and OLI imageries, the Fast Line-of-Sight Atmospheric Analysis of Spectral Hypercubes (FLAASH) model in ENVI 5.2 cannot correct the Landsat MSS imagery. Thus, the Landsat MSS digital numbers are corrected to pixel radiance according to the method described in the study of Markham and Barker 1986 and then corrected to TOA reflectance to extract lake body according to the radiometric specifications and the date of image acquisition (Lobo et al. 2015).

The modified normalized difference water index (MNDWI) (Xu 2006) was calculated for each Landsat TM, ETM+, and OLI image to identify and delineate HLL body. MNDWI (equation) can enhance open water features while efficiently suppressing and even removing built-up land noise as well as vegetation and soil noise (Xu 2006). The MNDWI is calculated as $[(\text{Green} - \text{MIR})/(\text{Green} + \text{MIR})]$, where MIR refers to the reflection in the middle infrared band, such as TM/ETM+ band 5 ($1.55\text{--}1.75 \mu\text{m}$) and OLI band 6 ($1.57\text{--}1.65 \mu\text{m}$); and Green refers to the reflection in the green band, such as TM/ETM+ band 2 ($0.52\text{--}0.60 \mu\text{m}$) and OLI band 3 ($0.53\text{--}0.59 \mu\text{m}$). Only the NDWI could be selected for the Landsat MSS image data due to insufficient middle infrared band. The NDWI is defined as $[(\text{Green} - \text{NIR})/(\text{Green} +$

NIR)] (McFeeters 1996) where NIR and Green represent the reflectance from the Landsat MSS data for band 7 (near-infrared band, $0.80\text{--}1.10 \mu\text{m}$) and band 4 (green band, $0.50\text{--}0.60 \mu\text{m}$). The threshold values of McFeeter's NDWI and Xu's MNDWI are zero. The threshold value of zero was also applied to extract water features from the MNDWI and NDWI images in this study.

The NDVI provides information about the spatial and temporal vegetation distribution and the extent of land degradation. This study uses the Global Inventory Modeling and Mapping Studies (GIMMS) Normalized Difference Vegetation Index third generation (NDVI3g) dataset, which was modified in September of 2016. The data quality and precision of GIMMS NDVI is higher than the other NDVI data and has been widely used in the global and regional vegetation change studies (Kobayashi and Dye 2005). The modified GIMMS NDVI products with a spatial resolution of 8 km by 8 km , from growing seasons (April–September) during 1981–2015, were compiled by merging segments (data strips) for half-month period using the maximum value composite (MVC) method. The method of MVC was also adopted to obtain the annual NDVI (annual NDVI = $\text{Max}(\text{NDVI}_{\text{M4}}, \text{NDVI}_{\text{M5}}, \dots, \text{NDVI}_{\text{M9}})$, where NDVI_{Mi} is the NDVI value of month i). We calculated the annual NDVI average of all the GIMMS NDVI3g pixels in the study area to indicate the general feature of NDVI variation with time.

The Standardized Precipitation Evapotranspiration Index (SPEI) considers the effect of reference evapotranspiration on drought severity, but the multi-scalar nature of the SPEI enables identification of different drought types and drought impacts on diverse systems (Vicente-Serrano et al. 2010). The SPEI uses the monthly (or weekly) difference between precipitation and potential evapotranspiration (PET). Vicente-Serrano (2010) selected the simplest approach to calculate PET (Thornthwaite 1948), which has the advantage of only requiring data on monthly mean temperature. The SPEI between 1960 and 2015 was calculated for the 1-month to 60-

month timescales by using monthly precipitation and air temperature data at Hailaer meteorological station.

The Global Land Data Assimilation System (GLDAS) is generating a series of land surface state and flux products simulated by four land surface models (CLM, Mosaic, Noah, and VIC) (Rodell et al. 2004). The GLDAS Noah model was forced by the combination of NOAA/GDAS atmospheric analysis fields, spatially and temporally disaggregated NOAA Climate Prediction Center Merged Analysis of Precipitation (CMAP) fields, and observation-based downward shortwave and longwave radiation fields derived using the method of the Air Force Weather Agency's Agricultural Meteorological system (see Rodell et al. 2004 for further details). The monthly soil moisture data at $0.25 \times 0.25^\circ$ in the GLDAS Noah dataset contain the depth-averaged amount of water present in the specific soil layer beneath the surface. In the Noah model, there are four soil layers which are located < 0.1 m, 0.1–0.4 m, 0.4–1.0 m, and 1.0–2.0 m below land surface. The soil moisture data used in this study included soil moisture average of all the 12 GLDAS Noah data pixels distributed in the study area (Fig. 1). The temporal coverage of GLDAS Noah Versions 2.0 and 2.1 are January 1948 to December 2010 and January 2000 to November 2018. The statistics from the pixel-by-pixel correlation between Versions 2.0 and 2.1 of GLDAS Noah data in the overlap period between January 2000 and December 2010 indicate the significant correlation of soil moisture data from Versions 2.0 and

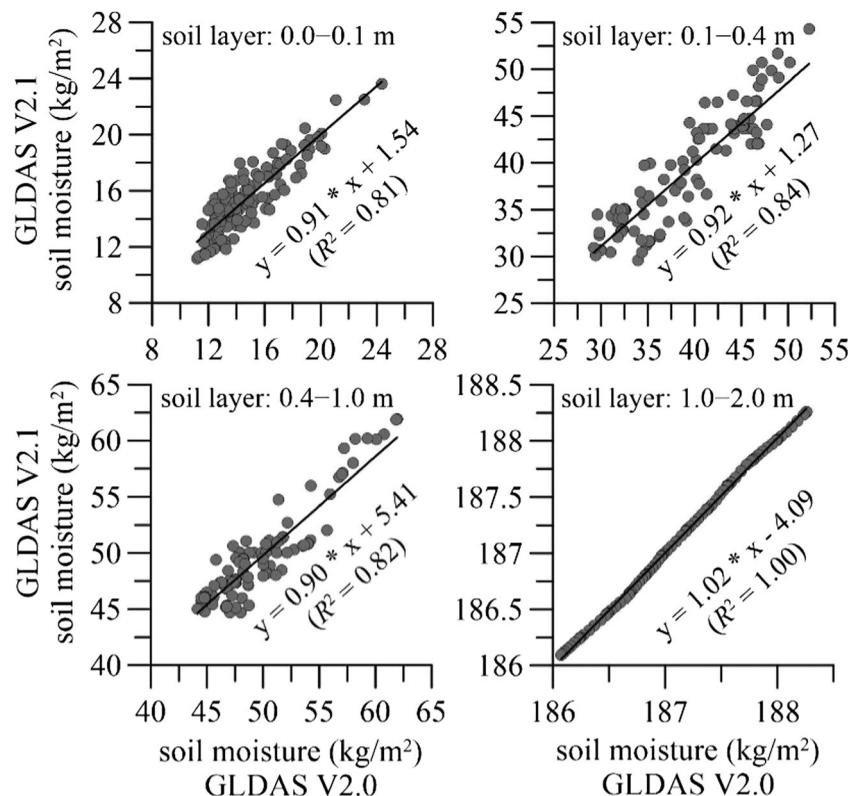
2.1 of GLDAS Noah data in the HLH area (Fig. 2) on the pixel scale; the absolute difference between them is mainly distributed among ± 8.4 . Given the significant correlation and the low absolute difference, the soil moisture data from GLDAS Versions 2.0 and 2.1 in this study area are consistent. Given the long period covered by the GLDAS dataset analyses, the soil moisture data from GLDAS Noah Version 2.0 with temporal coverage of January 1960 to December 1999 and the soil moisture data from GLDAS Noah Version 2.1 with temporal coverage of January 2000 to December 2015 were used. However, the data were not calibrated because of lack of available ground measurements with reliable quality for the calibration of the two datasets.

4 Results and discussion

4.1 Climate variation

The observed air temperature in the study area from 1960 to 2015 showed a mean annual average temperature (AAT) of -1.0°C , median AAT of -1.0°C , and minimum and maximum AAT since 1960 of -3.6°C in 1969 and 1.2°C in 2007. The AAT showed a decreasing trend over 1960–1966 and 2000–2009 and an increasing trend over 1967–1999 and 2010–2015 (Table 1). The minimum, maximum, and average annual precipitations (APs) from 1960 to 2015 were 124.5 mm in 1986,

Fig. 2 Comparison analysis of the soil moisture data from GLDAS V2.0 and V2.1



650.7 mm in 2013, and 350.4 mm (median = 340.85 mm), respectively. The AP fluctuated strongly over the past five decades, first decreasing and then increasing between 1960 and 1980 and then showing irregular distribution over 1981–2015 (Table 1). The annual average air relative humidity (AARH) in the study area from 1960 to 2015 varied from 57.5 to 73.6%, with an average of 66.6% (median = 67.4%). The AARH showed no consistent trend over 1960–2015 and fluctuated strongly over 1981–1989 and 1999–2015; these fluctuations could be related to irregular distribution of precipitation after 1981.

Seasonal precipitation has generally increased in winter and has been irregularly distributed in the other seasons since 1960. The percentage of seasonal precipitation in AP increased in winter over 1960–2015 and spring over 1981–2015, decreased in summer over 1960–2015, and became irregularly distributed in autumn over the last 55 years (Fig. 3). The ascending rates of the average temperatures in winter and spring (> 0.05 °C/a) were slightly higher than those in summer and autumn (0.04 °C/a) (Fig. 4). The decline rate of the average air relative humidity in summer and autumn was approximately 0.13%/a, which was higher than those in winter and spring (Fig. 5). Therefore, summer and autumn in the study area have become increasingly warmer and drier, and winter and spring have become increasingly warmer and relatively stable in terms of moisture since 1960.

Four climatic periods could be formed between 1960 and 2015 according to variation trends and multi-year averages of AAT and AP (Tables 1 and 2 and Fig. 6). Climatic stage 1 (1960 to 1979) is relatively cold and dry; its average AAT, AP, and AARH are -1.9 °C, 335.5 mm, and 67.1%, respectively. Climatic stage 2 (1980 to 1999) is warm and moist, and its average AAT, AP, and AARH are -0.7 °C, 369.7 mm, and 68.4%, respectively. Climatic stage 3 (2000 to 2009) is warm and dry, and its average AAT, AP, and AARH are 0.0 °C, 321.5 mm, and 63.2%, respectively. Climatic stage 4 (2010 to 2015) is cold and dry at the beginning, then become warm and moist, and its average AAT, AP, and AARH are -1.0 °C, 384.3 mm, and 64.9%, respectively. The highest AAT and AP and lowest AARH since 1960 are observed in climatic stages 3 and 4. To some extent, this finding shows that the study area experienced a more pronounced climate change in these periods than in the first two.

Table 1 Regression models for the relationship between precipitation/temperature and time

CS	Period	AP (p)	AAT (t)
1	1960–1966	$p = -15.94a + 31,609, R^2 = 0.38$	$t = -0.38a + 739.88, R^2 = 0.66$
	1967–1979	$p = 12.86a - 25,039, R^2 = 0.42$	$t = 0.06a - 119.46, R^2 = 0.35$
2	1980–1999	$p = 1.30a - 2221.7, R^2 = 0.00$	$t = 0.13a - 251.48, R^2 = 0.58$
3	2000–2009	$p = -3.67a + 7669.8, R^2 = 0.01$	$t = -0.10a + 196.71, R^2 = 0.27$
4	2010–20,158	$p = 20.15a - 40,165, R^2 = 0.07$	$t = 0.37a - 751.94, R^2 = 0.49$

CS, climatic stage; AAT, annual average temperature; AP, annual precipitation; a , year

4.2 Changes in HLL surface area and NDVI

Variations in the HLL area have shown a generally downward trend with several large fluctuations from 1960 to 2015 (Fig. 6). This timeline is divided into two increasing periods and two decreasing periods according to the HLL area variations (Table 3 and Fig. 6). The trend of NDVI with time showed a slight increase from 1981 to 1989 ($y = 0.01x - 21.77, R^2 = 0.31$) and then showed irregular distribution over 1990–2015. The vegetation cover was relatively high from 1981 to 1989, with an average or median NDVI of 0.53 (ranging from 0.42 to 0.61). In the next eight consecutive years (1990 to 1997), the average NDVI was 0.51 (ranging from 0.44 to 0.54) and dropped below the NDVI average in the last 35 years (Fig. 6). The vegetation improved from 1998 to 2015, with an average or median NDVI of 0.56 (ranging from 0.36 to 0.68). The NDVI values in the periods of 1990 to 1997 and 1998 to 2015 were irregularly distributed and showed no trend. The variations in the NDVI and the HLL area were different between 1981 and 2015. The NDVI values were relatively low from 1990 to 1997, while the HLL area expanded; the NDVI values were relatively high from 1982 to 1989 and from 2008 to 2014, while the HLL area shrank.

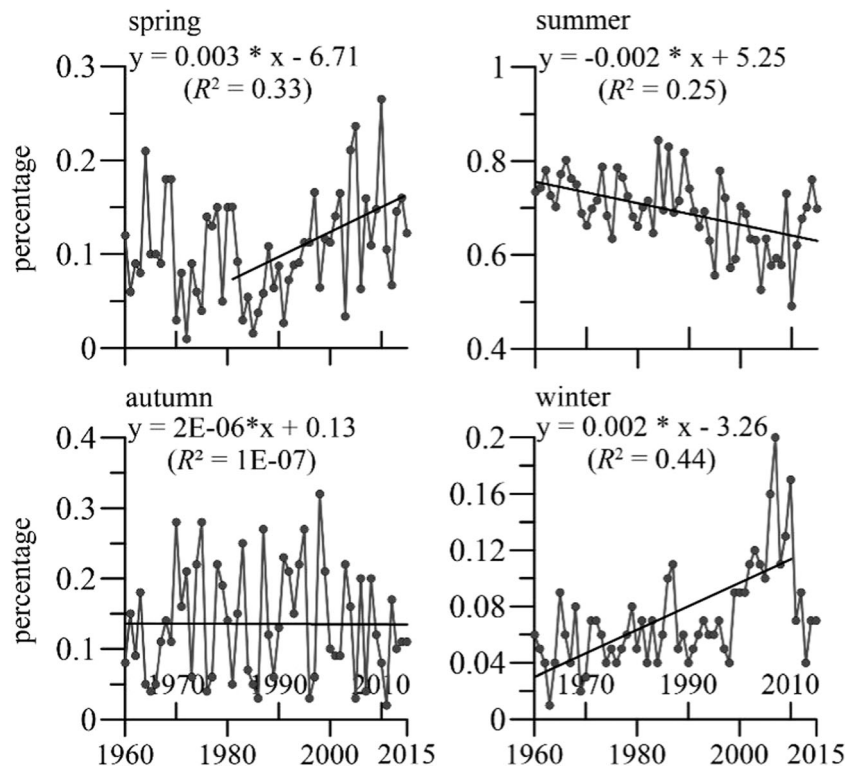
4.3 Impact of climate-related factors on changes in lake area

4.3.1 Precipitation, temperature, and relative humidity

The HLL area variation was gradually decreasing in the cold and rainless climatic stage 1 from 1960 to 1979. However, in the warm and moist climatic stage 2 from 1980 to 1999, the HLL area showed a sharp increase. In climatic stage 3 from 2000 to 2009, the climate was warm and dry most of the time, and the area variation of HLL had a strongly shrinking trend. The AP, AAT, and AARH fluctuated in climatic stage 4 from 2010 to 2015, and the area variation of HLL showed the second increasing trend since 1960.

During two periods of HLL shrinking (climatic stages 1 and 3), AP was generally lower than the historical precipitation average of 350.4 mm from 1960 to 2015 (Fig. 6). AP was lower than 350.4 mm for 12 and 10 years during the two periods of HLL shrinking, which were from 1963 to 1975

Fig. 3 The temporal trends of the percentage of seasonal precipitation in the annual precipitation during 1960–2015



(climatic stage 1) and from 2000 to 2012 (climatic stage 3), and the average APs in these two periods were only 347.4 (median = 337.7 mm) and 318.8 mm (median = 318.4 mm), respectively. The long-term and low amount of precipitation

in the HLL and the surrounding catchment was the main cause of the shrinking of the HLL in the past five decades. In long and generally rainless periods, the HLL area responded weakly to increases in precipitation with the short-term amount. For

Fig. 4 The temporal trends of seasonal air temperature during 1960–2015

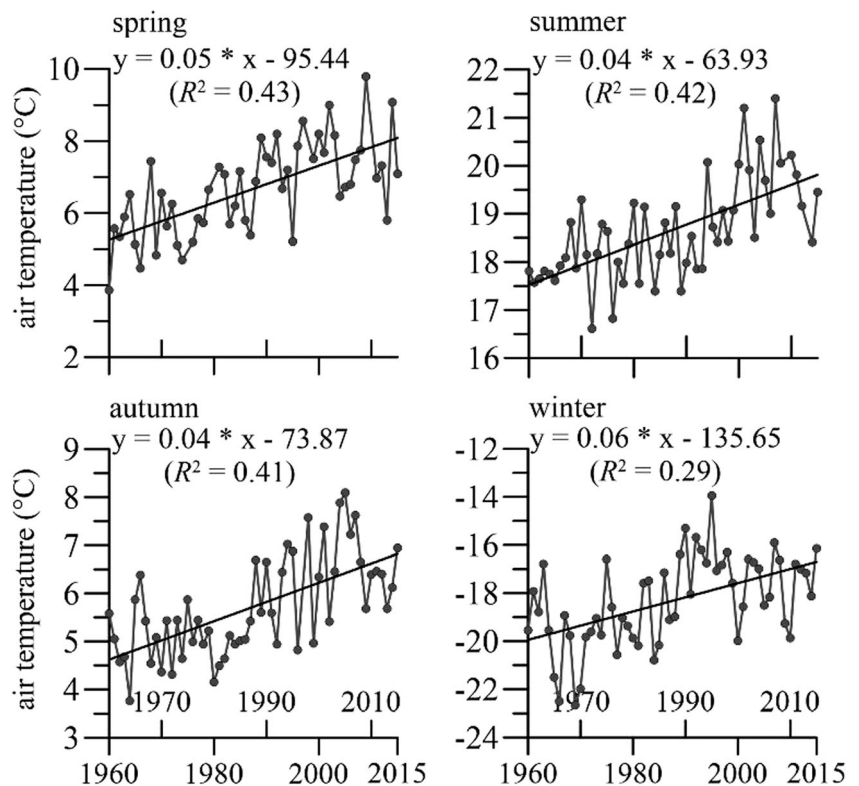
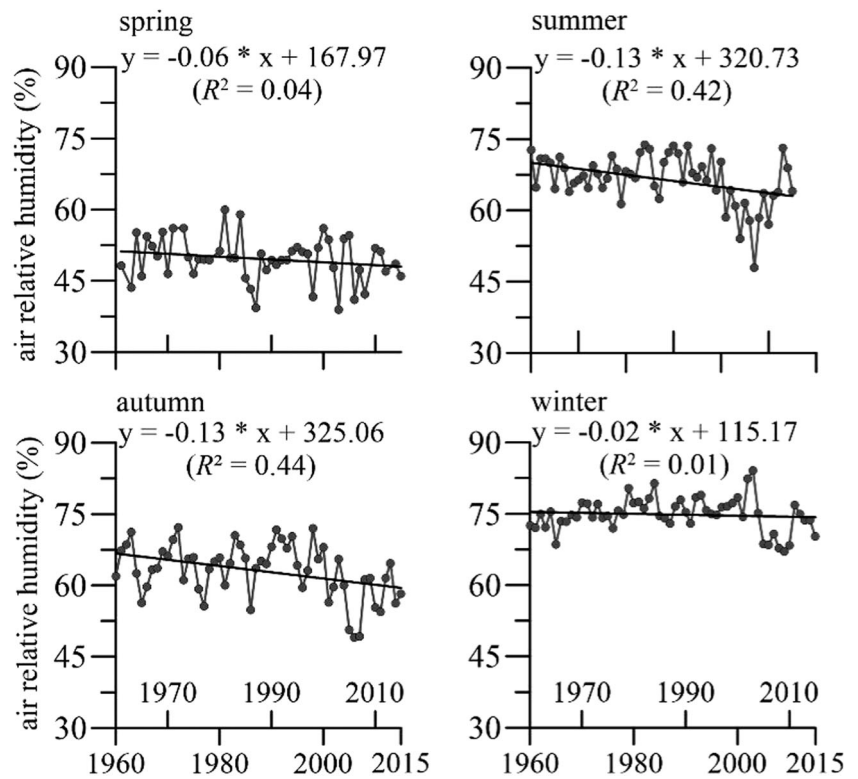


Fig. 5 The temporal trends of seasonal air relative humidity during 1960–2015



instance, AP was high in several scattered years (1976, 1977, 1982, and 1984) in the first period of HLL shrinking since 1960, but the HLL area itself showed a stable shrinking trend without obvious fluctuations in those scattered rainy years.

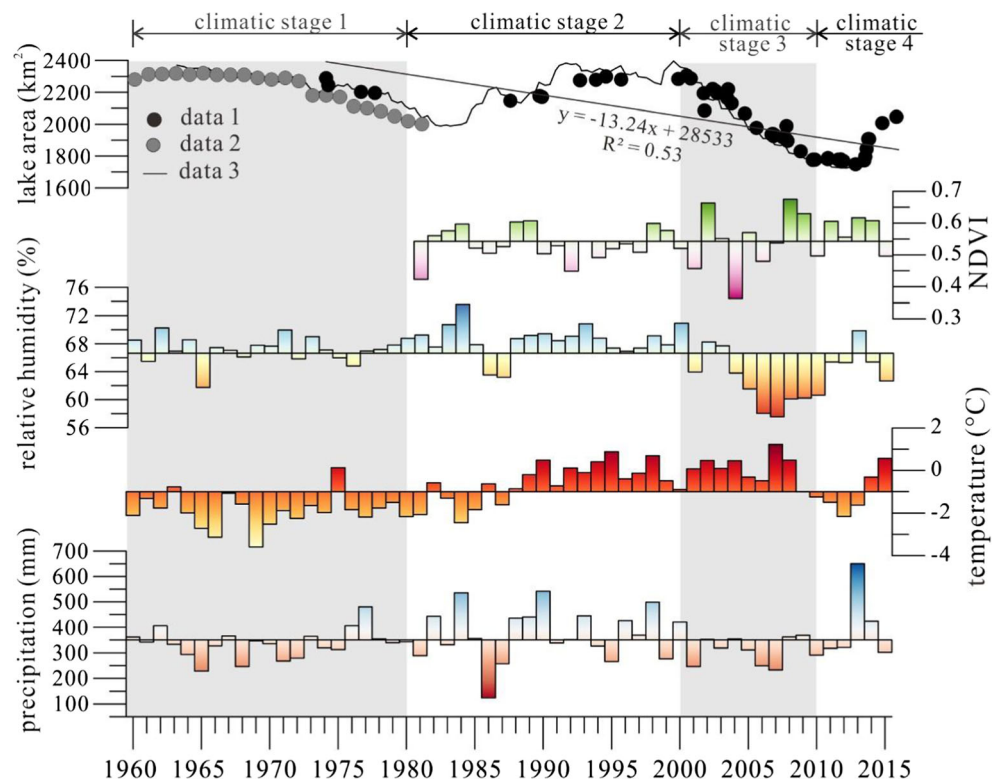
Variations in the lake area and precipitation were not always consistent because other climatic factors, such as air temperature and relative humidity, can also affect the lake area by enhancing or weakening its response to precipitation changes. The HLL region experienced rainless years from

1960 to 1969, but the HLL areas were stable at 2307 km² (ranging from 2280 to 2320 km²). This observation resulted from the decreasing lake evaporation caused by the continuous reduction of AAT from 1960 to 1969 (Fig. 6). In addition, although the average AP in the first shrinking period of HLL from 1970 to 1983 increased compared with that from 1960 to 1969, the area of the HLL still decreased from 1970 to 1983. This finding could be related to the increased lake evaporation caused by the rising average of AAT from -2.0 °C from 1960

Table 2 The variations in climatic factors over the past 55 years

	Climatic stage	Temperature					Precipitation					Relative humidity				
		Spring	Summer	Autumn	Winter	AAT	Spring	Summer	Autumn	Winter	AP	Spring	Summer	Autumn	Winter	AARH
1	Avg.	5.9	18.0	5.1	-19.7	-1.9	33.5	240.9	44.4	16.7	335.5	50.7	67.6	64.3	74.5	67.1
	Min.	3.9	16.6	3.8	-23.3	-3.6	2.1	147.6	8.0	4.9	228.3	39.9	61.4	55.7	68.6	61.8
	Max.	8.4	19.3	6.4	-16.6	0.1	63.7	367.4	94.1	26.4	480.1	58.9	72.8	72.2	80.4	70.3
2	Avg.	6.9	18.4	5.5	-17.6	-0.7	34.3	258.6	55.4	21.5	369.7	49.6	69.2	65.8	76.4	68.4
	Min.	3.7	16.7	4.2	-20.8	-2.5	4.7	103.4	3.9	12.5	124.5	39.4	62.4	54.8	72.9	63.2
	Max.	9.7	20.1	7.6	-14.0	0.9	99.1	451.9	159.4	31.7	541.7	60.0	73.8	72.1	81.4	73.6
3	Avg.	7.8	19.8	6.9	-17.7	0.0	40.0	203.3	40.5	37.7	321.5	47.2	59.7	58.1	73.7	63.2
	Min.	6.5	17.7	5.4	-20.0	-1.0	8.1	137.9	8.8	21.2	232.5	36.6	47.9	49.1	67.1	57.5
	Max.	9.8	21.4	8.1	-15.9	1.2	74.7	295.8	73.7	47.5	420.6	56.1	70.2	68.1	84.1	70.9
4	Avg.	7.0	19.2	6.3	-19.5	-1.0	47.9	267.3	38.9	29.6	384.3	50.9	65.0	58.4	73.0	64.9
	Min.	5.6	17.9	5.7	-22.2	-2.2	21.4	142.9	7.7	20.3	290.9	46.0	57.0	54.4	68.4	60.6
	Max.	9.1	20.2	7.0	-16.1	0.6	94.7	456.6	68.0	49.0	650.7	60.8	73.1	64.6	76.9	69.9

Fig. 6 Fluctuations in annual precipitation (AP), temperature (AAT), relative humidity (AARH), NDVI, and HLH area. Baselines of the floating bars represent the average data of AP, AAT, AARH, and NDVI from 1960 to 2015. Data 1 represents the lake area identified and measured based on Landsat images in this study; data 2 and 3 represent the lake area calculated by the area-level relationship, and the sources of lake level include in situ measurement (data 2, Zhang et al. 1998) and model prediction (data 3, Cai et al. 2016)



to 1969 to -1.7°C from 1970 to 1983. Moreover, the different rates of shrinking of the lake area between the rainless periods of 1970 to 1983 and 2000 to 2012 were also related to the evidently higher AAT and lower AARH from 2000 to 2012 than from 1970 to 1982.

The influences of seasonal precipitation, temperature, and relative humidity variations during the last half-century on the HLL area were different. The HLL area was stable in winter because the lake was covered by ice and the evaporation and recharge from precipitation were weak. However, the lake area normally enlarged in spring as the increasing runoff of melted water into the lake and the relatively low temperature led to low levels of lake evaporation. The fluctuations in the HLL area in summer and autumn were large in different periods, and the fluctuations mainly depended on lake evaporation and precipitation (including direct recharge and runoff).

Pearson's correlation coefficients of the HLL area and annual climatic factors (AP, AAT, and AARH) are generally lower than 0.54 ($p < 0.01$). The variations in the HLL area over the past half-century were strongly and comprehensively

influenced by the long-term (several years or even longer) variation trends of climatic factors. If the long-term AAT were higher or lower than its multi-year average from 1960 to 2015, a decrease or increase in AP could rapidly result in the reduction or expansion of the lake area. Otherwise, the response sensitivity of the lake area to AP would be reduced and a response lag may appear.

4.3.2 SPEI and soil moisture

We evaluated the response of the HLL area to drought by correlating a drought index (SPEI). SPEI can incorporate the effect of hydrological balance between precipitation and potential evapotranspiration, which is sensitive to air temperature. An analysis of the SPEI timescales where the maximum correlations were recorded reveals that the HLL area responded predominantly to long timescales of drought (Figs. 7 and 8). That is, the lake area reacted strongly only when the lake experienced multi-year water deficits (precipitation minus potential evapotranspiration) below normal

Table 3 The variation of the Hulun Lake area over the past 55 years

No.	Period	Area variation (km^2)	Rate of variation (km^2/a)
1	1960–1979	2339–2080	-12.95 ($y = -12.921x + 27,702$, $R^2 = 0.67$)
2	1980–1999	2080–2304	11.26 ($y = 11.26x - 20,207$, $R^2 = 0.70$)
3	2000–2009	2304–1746	-54.39 ($y = 54.39x + 111,100$, $R^2 = 0.67$)
4	2010–2015	1746–2047	52.69 ($y = 52.69x - 104,213$, $R^2 = 0.67$)

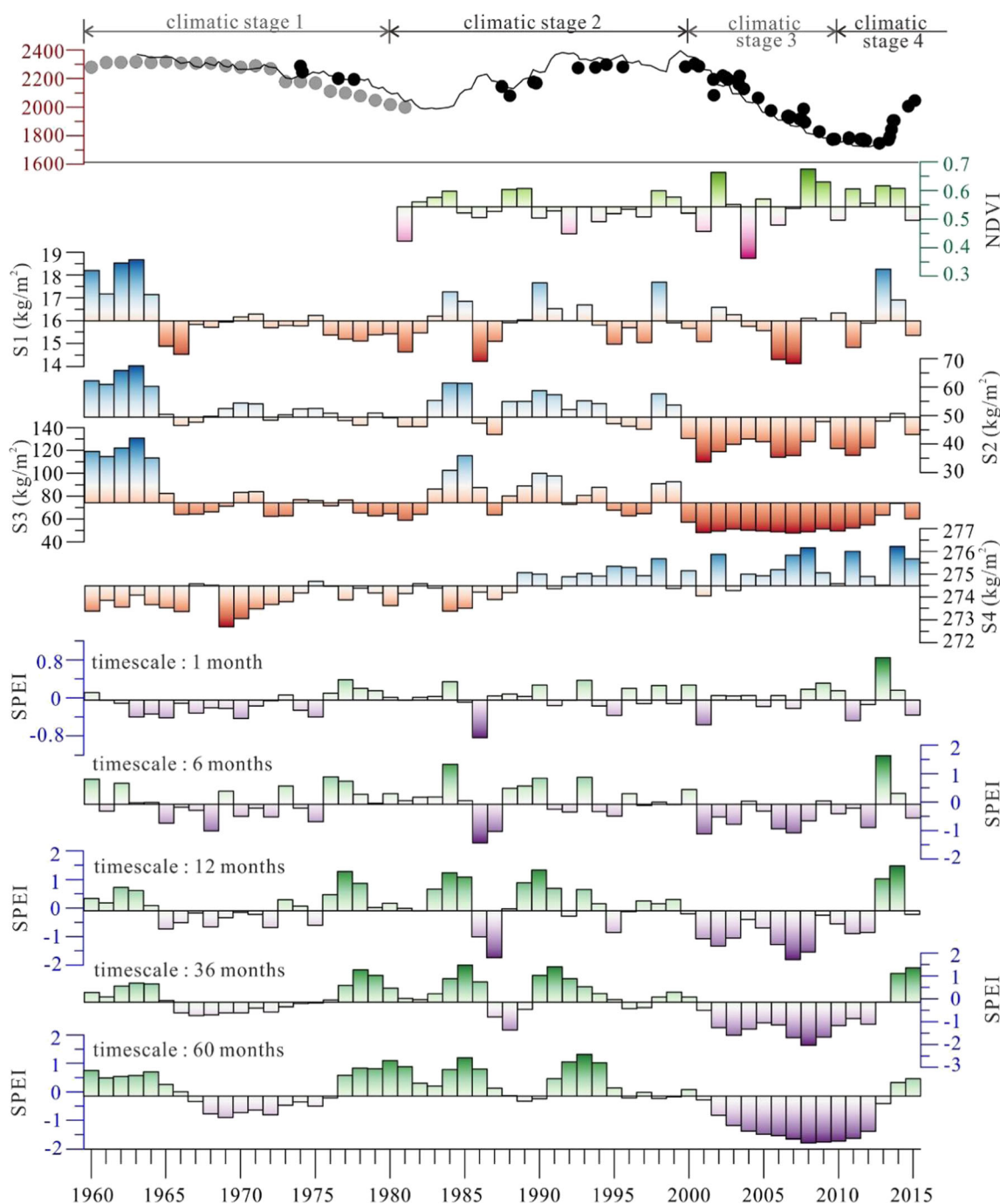


Fig. 7 Fluctuations in SPEI with different timescales, soil moisture at different depths, NDVI, and HLH area. Baselines of the floating bars indicate the average data of SPEI, soil moisture, and NDVI from 1960 to 2015. S1, S2, S3, and S4 represent soil moisture at depths of <0.1 m, 0.1–0.4 m, 0.4–1.0 m, and 1.0–2.0 m, respectively

conditions. The relatively weak correlations between the HLL area and SPEI with timescales of less than 5 years ($r = -0.32$ to 0.47) confirm that the HLL area strongly responded to climatic factors at long timescales. From 1960 to 2015, Pearson’s correlation coefficients of the HLL area and the SPEI with a 5-year timescale are in the following order: 0.58 ($p < 0.01$) in spring, > 0.55 ($p < 0.01$) in winter, > 0.51

($p < 0.01$) in summer, > 0.44 ($p < 0.01$) in autumn. These figures suggest that the HLL area was more closely related to the spring and winter SPEI variations, which could be used as an indicator to detect changes in the lake area. The relatively weak correlations between HLL area and summer or autumn SPEI indicate the complexity of the factors that affect the lake area variation. Meanwhile, the differences between the

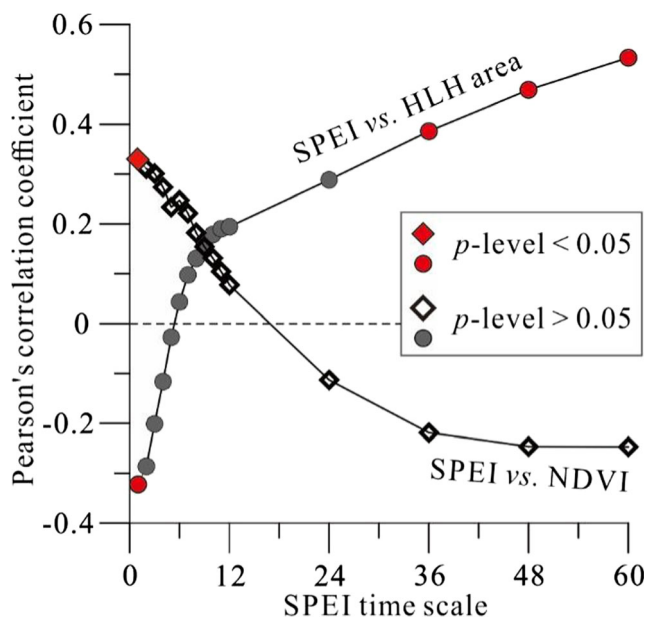


Fig. 8 Relationships between the SPEI and lake area/NDVI over 1960–2015

hydrological balance represented by SPEI and the actual balance of recharge and discharge in HLL were larger in summer and autumn than those in spring and winter.

Soil moisture is also directly affected by precipitation and evapotranspiration and can profoundly influence the lake area and NDVI. Pearson's correlation coefficients of AP/evapotranspiration and soil moistures in different soil layers in the study area gradually decrease from 0.56 ($p < 0.01$)/0.57 ($p < 0.01$) in the first 0.0 to 0.1 m of soil to 0.10 ($p > 0.05$)/0.30 ($p < 0.05$) from 1.0 to 2.0 m of soil below the land surface. The AAT is weakly correlated with soil moisture at depths of < 1.0 m ($r < 0.27$, $p < 0.01$) and strongly correlated with soil moisture in the deep layer (1.0 to 2.0 m; $r = 0.78$, $p < 0.01$). These findings indicate that precipitation and evapotranspiration mainly influenced the soil moisture in the shallow layer, and groundwater evaporation affected by temperature variations could evidently influence the soil moisture in the deep layer. Figure 9 shows the correlation variations of the HLL area and soil moistures at different depths from 1960 to 2015 and indicates a more positive correlation between the HLL area and soil moisture of seasonal and annual averages at depths of 0.4 to 1.0 m than those at other soil depths. This result confirms that the soil moisture at depths of 0.4 to 1.0 m and the HLL area were closely related and had similar responses to climatic change. Soil moisture at depths of 0.4 to 1.0 m in winter and spring and the annual average could be used as potential indicators for predicting the variation tendency of the HLL area. The negative correlation between the HLL area and soil moisture in the deep layer (> 1.0 m) could be caused by the different influences of groundwater on the lake water and soil moisture in the study area. During the hot and dry periods, the soil water in the deep layer of the study area

could be recharged by the evaporation of shallow groundwater, but the HLL area would decrease because of the lake water evaporation and because the recharge of groundwater into HLL was limited by the deep sludge aquiclude in the lake bottom.

4.4 Impact of climate-related factors on changes in NDVI

4.4.1 Precipitation, temperature, and relative humidity

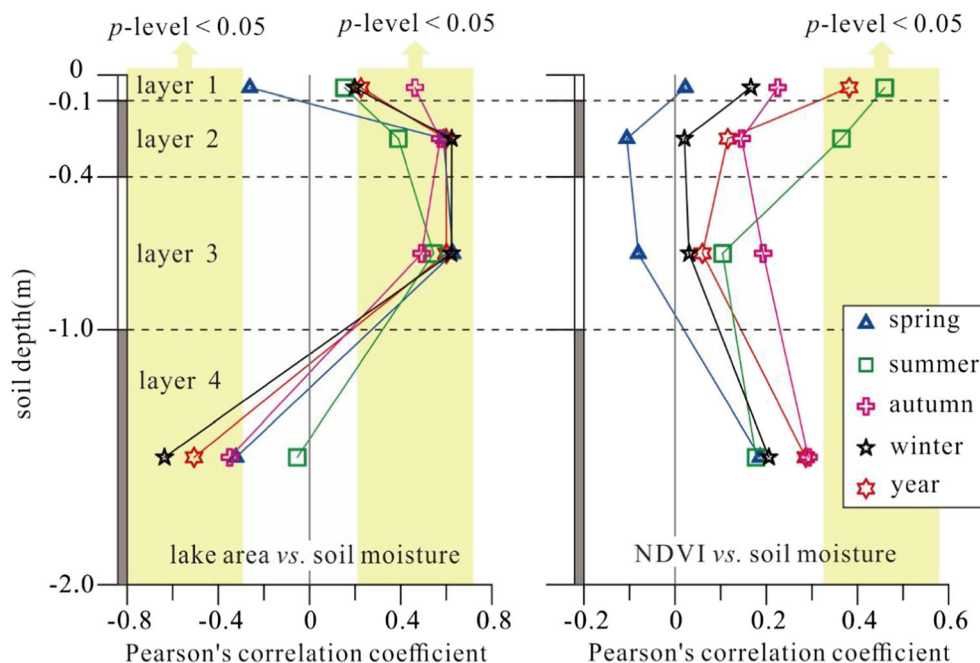
The study area showed a low NDVI in the eight consecutive years from 1990 to 1997, but the AP and seasonal precipitation in most of these years were higher than their historical averages from 1960 to 2015 (Fig. 6). Furthermore, HLL was expanding from 1990 to 1999 as the main water source for local vegetation. Thus, the low NDVI in the study area could not have resulted from water restriction. Further research shows that the low vegetation cover from 1990 to 1999 was probably related to the intense grazing before the local law enforcement of the grazing prohibition in the Dalai Hu National Nature Reserve in 1998. The grazing prohibition in this area from 1998 to 2015 promoted vegetation restoration.

An analysis of NDVI–climate relationships reveals Pearson's correlation coefficient of 0.37 ($p < 0.01$) for NDVI–AP, which is higher than those of NDVI–AAP and NDVI–AARH. Regarding seasonal climate factors, summer precipitation and NDVI show the highest Pearson's correlation coefficient of 0.39 ($p < 0.05$). This result suggests that AP, especially summer precipitation, had an important influence on the vegetative growth in the study area. Between 1998 and 2015, when grazing had already been eliminated, Pearson's correlation coefficient of NDVI and summer precipitation increases to 0.45 ($p < 0.05$), which is still higher than those in the other seasons. Pearson's correlation coefficients of the NDVI and seasonal temperature means are 0.47 ($p < 0.05$) in spring, -0.45 ($p < 0.05$) in summer, -0.55 ($p < 0.05$) in autumn, and -0.03 ($p > 0.05$) in winter. Hence, increasing spring temperature and decreasing summer and autumn temperatures could increase the NDVI. This finding is consistent with the study of Chuai (2013), who implied that the NDVI is negatively correlated with temperature and positively correlated with precipitation for cultivated vegetation, shrubs, steppes, meadows, and desert vegetation in summer in Inner Mongolia. The differences in the observed relationships can be explained by the fact that the demand for heat varied among different seasons and the temperatures are too high or too low to inhibit vegetation growth.

4.4.2 SPEI and soil moisture

Pearson's correlation coefficients of NDVI and SPEI gradually decrease from 0.33 ($p < 0.05$) to -0.25 ($p > 0.05$) with the

Fig. 9 Relationships between the soil moistures and lake area/NDVI over 1960–2015



increase of SPEI timescales from 1 month to 5 years (Fig. 8). The variation trends of Pearson's correlation coefficients in Fig. 8 suggest that the sensitivities of NDVI and HLL area variation to the SPEI with different timescales were different. A drought in a short timescale (such as 1 month) could affect NDVI prominently because vegetation cover would first decrease rapidly and then maintain a slow rate with small fluctuations in a large timescale of drought. However, the HLL area changed with long-term drought (such as several years).

Pearson's correlation coefficients of NDVI and annual or seasonal soil moisture averages in shallow depths (<0.1 m) are higher than those in the middle and deep layers (0.1–2.0 m, Fig. 9). In the period of 1998 to 2015, without the grazing influence, Pearson's correlation coefficient of NDVI and shallow soil moisture (<0.1 m) rises to 0.43 ($p < 0.05$). The shallow soil moisture at the depth of <0.1 m shows highest Pearson's correlation coefficient with the NDVI (0.46, $p < 0.01$) through all four seasons. Furthermore, in all the four soil layers with depths <2.0 m, the correlations of NDVI and soil moisture are generally weaker than the correlation between HLL area and soil moisture. The depth of the soil layer with highest Pearson's correlation coefficient of soil moisture and NDVI is lower than that of the soil layer with highest Pearson's correlation coefficient of soil moisture and HLL area. This result indicates that the soil moisture of the shallow soil layer (<0.1 m), which is the first and most sensitively affected layer by precipitation, evaporation, and other climate-related variables, could largely influence the vegetation cover because the soil moisture in the shallow depth (<0.1 m) was the key root-zone soil moisture in the study area that could influence NDVI. The soil moisture in the shallow layer could also affect the HLL area, but the influence of soil

moisture on the HLL area was stronger in the deep soil layer with depths between 0.4 and 1.0 m.

5 Conclusion

The climate in the Hulun Buir Grassland of Northeastern China has fluctuated largely over the past 55 years and has led to the variation in HLL area in the range of 1746 to 2339 km². The amount of precipitation in a long timescale (several years or even longer) is the key factor that controls lake area variation, but an increase or decrease in the air temperature and relative humidity could affect the response time of the HLL area to precipitation. The amount of precipitation, especially summer precipitation, was the primary climatic factor that affected the vegetation cover in the study area. Meanwhile, increasing spring temperature and decreasing summer and autumn temperatures could increase the NDVI values.

Pearson's correlation coefficients of the HLL area and the SPEI show that the HLL area becomes more closely related with the SPEI as the timescale of SPEI increases. However, the NDVI values in this study are positively correlated with the monthly timescale of SPEI. Furthermore, the moisture averages of the soil layer at the depths of 0.4–1.0 and <0.1 m show the highest correlations with the HLL area and NDVI, respectively. This finding indicates that soil moisture in the shallow depths (<0.1 m) was the key root-zone soil moisture that could influence NDVI, whereas the soil moisture at the depths of 0.4–1.0 m and the HLL area were closely related and responded similarly to climatic change.

Acknowledgements We thank the anonymous reviewers for their comments that resulted in a greatly improved manuscript.

Funding information This study was financially supported by the Fundamental Research Fund of the China Institute of Water Resources and Hydropower Research (MK2017J01 and MK2016J15) and the National Natural Science Foundation of China (No. 41807215).

Publisher's note Springer Nature remains neutral with regard to jurisdictional claims in published maps and institutional affiliations.

References

- Ashraf A, Naz R, Iqbal MB (2017) Altitudinal dynamics of glacial lakes under changing climate in the Hindu Kush, Karakoram, and Himalaya ranges. *Geomorphology* 283:72–79
- Bai J, Chen X, Li JL, Yang L, Fang H (2011) Changes in the area of inland lakes in arid regions of central Asia during the past 30 years. *Environ Monit Assess* 178(1–4):247–256
- Bao G, Qin ZH, Bao YH, Zhou Y, Li WJ, Sanjiv A (2014) NDVI-based long-term vegetation dynamics and its response to climatic change in the Mongolian Plateau. *Remote Sens* 6(9):8337–8358
- Cai ZS, Jin TY, Li CY, Ofterdinger U, Zhang S, Ding A-Z, Li JC (2016) Is China's fifth-largest inland lake to dry-up? Incorporated hydrological and satellite-based methods for forecasting Hulun lake water levels. *Adv Water Resour* 94:185–199
- Chuai XW, Huang XJ, Wang WJ, Bao, G (2013) NDVI, temperature and precipitation changes and their relationships with different vegetation types during 1998–2007 in Inner Mongolia, China. *Int J Climatol* 33(7):1696–1706
- Debnath M, Syiemlieh HJ, Sharma MC, Kumar R, Chowdhury A, Lal U (2018) Glacial lake dynamics and lake surface temperature assessment along the Kangchengayo-Pauhunri Massif, Sikkim Himalaya, 1988–2014. *RSASE* 9:26–41
- Fang L, Tao S, Zhu J, Liu Y (2018) Impacts of climate change and irrigation on lakes in arid northwest China. *J Arid Environ* 154:34–39
- Gong DY, Ho CH (2003) Detection of large-scale climate signals in spring vegetation index (normalized difference vegetation index) over the Northern Hemisphere. *J Geophys Res Atmos* 108:D16
- Gong DY, Shi PJ (2004) Inter-annual changes in Eurasian continent NDVI and its sensitivity to the large-scale climate variations in the last 20 years. *Acta Bot Sin* 46(2):186–193
- Im ST, Kharuk VI, Rakityanskaya NM, Golyukov AS (2015) Climate-induced lake dynamics in the Trans-Baikal forest-steppe ecotone. *Contemp Probl Ecol* 8(6):680–686
- Jing Y, Zhang F, Wang X (2018) Monitoring dynamics and driving forces of lake changes in different seasons in Xinjiang using multi-source remote sensing. *EuJRS* 51(1):150–165
- Jones BM, Grosse GD, Arp CD, Jones MC, Anthony KW, Romanovsky VE (2011) Modern thermokarst lake dynamics in the continuous permafrost zone, northern Seward Peninsula, Alaska. *J Geophys Res Biogeosci* 116(G2)
- Kaiser K, Heinrich I, Heine I, Natkhin M, Dannowski R, Lischeid G (2015) Multi-decadal lake-level dynamics in north-eastern Germany as derived by a combination of gauging, proxy-data and modelling. *J Hydrol* 529:584–599
- Kang S, Lee G, Togtokh C, Jang K (2015) Characterizing regional precipitation-driven lake area change in Mongolia. *J Arid Land* 7(2):146–158
- Karlsson JM, Lyon SW, Destouni G (2014) Temporal behavior of lake size-distribution in a thawing permafrost landscape in Northwestern Siberia. *Remote Sens* 6(1):621–636
- Kobayashi H, Dye DG (2005) Atmospheric conditions for monitoring the long-term vegetation dynamics in the Amazon using normalized difference vegetation index. *Remote Sens Environ* 97(4):519–525
- Li C, Sun B, Jia K, Zhang S, Li WP (2013) Multi-band remote sensing based retrieval model and 3D analysis of water depth in Hulun Lake, China. *Math Comput Model* 58(3–4):765–775
- Lobo FL, Costa MP, Novo EM (2015) Time-series analysis of Landsat-MSS/TM/OLI images over Amazonian waters impacted by gold mining activities. *Remote Sens Environ* 157:170–184
- Lu N, Wilske B, Ni J, John R, Chen J (2009) Climate change in Inner Mongolia from 1955 to 2005—trends at regional, biome and local scales. *Environ Res Lett* 4(4):45006–45006
- Markham BL, Barker JL (1986) Landsat MSS and TM post-calibration dynamic rangers, exoatmospheric reflectance and at-satellite temperatures. *Landsat Technical Notes* 3–8
- McFeeters SK (1996) The use of the Normalized Difference Water Index (NDWI) in the delineation of open water features. *Int J Remote Sens* 17(7):1425–1432
- Nitze I, Grosse G, Jones BM, Arp CD, Ulrich M, Fedorov A, Veremeeva A (2017) Landsat-based trend analysis of lake dynamics across northern permafrost regions. *Remote Sens* 9(7):640
- Olthof I, Fraser RH, Schmitt C (2015) Landsat-based mapping of thermokarst lake dynamics on the Tuktoyaktuk Coastal Plain, Northwest Territories, Canada since 1985. *Remote Sens Environ* 168:194–204
- Piao SL, Mohammad A, Fang JY, Cai Q, Feng JM (2006) NDVI-based increase in growth of temperate grasslands and its responses to climate changes in China. *Glob Environ Chang* 16(4):340–348
- Polishchuk YM, Sharonov DS (2013) Studying the dynamics of thermokarst lake fields in Altai mountain valleys. *Izvestiya, Atmospheric and Oceanic Physics* 49(9):1074–1077
- Prentice IC (2001) Interactions of climate change and the terrestrial biosphere. *Geosphere-biosphere interactions and climate*. Cambridge University Press, New York
- Qian WH, Lin X (2004) Regional trends in recent temperature indices in China. *Clim Res* 27(2):119–134
- Qin DH, Ding YH, Su JL, Ren JW (2005) Assessment of climate and environment changes in China (I): climate and environment changes in China and their projection. *Adv Clim Chang Res* 1(1):4–9
- Rodell M, Houser PR, Jambor U, Gottschalk J, Mitchell K, Meng CJ, Arsenault K, Cosgrove B, Radakovich J, Bosilovich M, Entin JK, Walker JP, Lohmann D, Toll D (2004) The global land data assimilation system. *Bull Am Meteorol Soc* 85(3):381–394
- Smith LC, Sheng Y, MacDonald GM, Hinzman LD (2005) Disappearing arctic lakes. *Science* 308(5727):1429–1429
- Sun YL, Guo P, Yan XD, Zhao TB (2010) Dynamics of vegetation cover and its relationship with climate change and human activities in Inner Mongolia. *J Nat Resour* 25(3):407–414
- Tao S, Fang J, Zhao X, Zhao S, Shen H, Hu H, Tang Z, Wang Z, Guo Q (2015) Rapid loss of lakes on the Mongolian Plateau. *Proc Natl Acad Sci* 112(7):2281–2286
- Thornthwaite CW (1948) An approach toward a rational classification of climate. *Geogr Rev* 38(1):55–94
- Tucker CJ, Slayback DA, Pinzon JE, Los SO, Myneni RB, Taylor MG (2001) Higher northern latitude normalized difference vegetation index and growing season trends from 1982 to 1999. *Int J Biometeorol* 45(4):184–190
- Vallet-Coulomb C, Legesse D, Gasse F, Travi Y, Chernet T (2001) Lake evaporation estimates in tropical Africa (Lake Ziway, Ethiopia). *J Hydrol* 245(1–4):1–18
- Vicente-Serrano SM, Beguería S, López-Moreno JI (2010) A multiscalar drought index sensitive to global warming: the standardized precipitation evapotranspiration index. *J Clim* 23(7):1696–1718
- Wang J, Rich PM, Price KP (2003) Temporal responses of NDVI to precipitation and temperature in the central Great Plains, USA. *Int J Remote Sens* 24(11):2345–2364

- Wang J, Sheng Y, Tong TSD (2014) Monitoring decadal lake dynamics across the Yangtze Basin downstream of Three Gorges Dam. *Remote Sens Environ* 152:251–269
- Xiao J, Chang Z, Wen R, Zhai D, Itoh S, Lomtatidze Z (2009) Holocene weak monsoon intervals indicated by low lake levels at Hulun Lake in the monsoonal margin region of northeastern Inner Mongolia, China. *The Holocene* 19(6):899–908
- Xing L, Tang X, Wang H, Fan W, Wang G (2018) Monitoring monthly surface water dynamics of Dongting Lake using Sentinel-1 data at 10 m. *PeerJ* 6:e499
- Xu HQ (2006) Modification of normalised difference water index (NDWI) to enhance open water features in remotely sensed imagery. *Int J Remote Sens* 27(14):3025–3033
- Xu Z-J, Jiang F-Y, Zhao H-W, Zhang Z-B, Sun L (1989) *Annals of Hulun Lake*. Jilin Literature and History Publishing House, Changchun
- Yang K, Yao F, Wang J, Luo J, Shen Z, Wang C, Song C (2017) Recent dynamics of alpine lakes on the endorheic Changtang Plateau from multi-mission satellite data. *J Hydrol* 552:633–645
- Yao J, Chen Y, Zhao Y, Yu X (2018) Hydroclimatic changes of Lake Bosten in Northwest China during the last decades. *Sci Rep* 8(1):9118
- Zhang Z, Jiang F, Wang S, Yu S, Jiang M (1998) *Continuation of Annals of Hulun Lake*. Inner Mongolia Culture Publishing House, Hohhot
- Zhang BW, Cui LL, Shi J, Wei PP (2017) Vegetation dynamics and their response to climatic variability in China. *Adv Meteorol* 2017(14):1–10